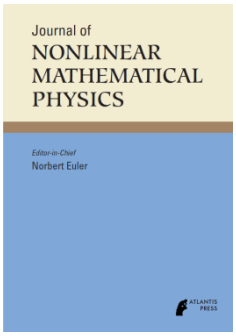

ATLANTIS PRESS

Journal of Nonlinear Mathematical Physics

ISSN (Online): 1776-0852 **ISSN (Print): 1402-9251**
Journal Home Page: https://www.atlantis-press.com/journals/jnmp

Solitary Waves in Open Channels with Abrupt Turns and Branching Points

André Nachbin, Vanessa da Silva Simões

To cite this article: André Nachbin, Vanessa da Silva Simões (2012) Solitary Waves in Open Channels with Abrupt Turns and Branching Points, Journal of Nonlinear Mathematical Physics 19:Supplement 1, 116–136, DOI: https://doi.org/10.1142/S1402925112400116

To link to this article: https://doi.org/10.1142/S1402925112400116

Published online: 04 January 2021

ARTICLE

World Scientific
www.worldscientific.com

ATLANTIS PRESS

Journal of Nonlinear Mathematical Physics, Vol. 19, Suppl. 1 (2012) 1240011 (21 pages)

DOI: 10.1142/S1402925112400116

SOLITARY WAVES IN OPEN CHANNELS WITH ABRUPT TURNS AND BRANCHING POINTS

ANDRÉ NACHBIN* and VANESSA DA SILVA SIMÕES†

Instituto Nacional de Matemática Pura e Aplicada
Est. D. Castorina, 110, Rio de Janeiro, RJ, 22460-320 Brazil
**nachbin@impa.br*
†*vanessasimoes@gmail.com*

Received 4 April 2012
Accepted 30 May 2012
Published 28 November 2012

The dynamics of solitary waves is studied in intricate domains such as open channels with sharp-bends and branching points. Of particular interest, the wave characteristics at sharp-bends is rationalized by using the Jacobian of the Schwarz–Christoffel transformation. It is observed that it acts in a similar fashion as a topography in other wave models previously studied. Previous numerical studies are revisited. A new very efficient algorithm is described, which computationally solves the problem in much more general channel configurations than presented in the literature. Also the conformal mapping naturally leads to a new strategy regarding the geometrical singularity at the sharp-bends. Finally preliminary results illustrate the use of the mapping's Jacobian at a channel's branching point. A future goal of this study regards deducing accurate reduced (one-dimensional) models for the reflection and transmission of solitary waves on graphs/networks.

Keywords: Water waves; solitary waves; tsunami in channels.

Mathematics Subject Classification 2000: 22E46, 53C35, 57S20

1. Introduction

The propagation of nonlinear waves in highly curved open channels, which may have branching points, is a problem of great interest. To mention a few, the applications range from flood and tidal waves in rivers, to channels of an irrigation network, and even tsunamis in Norwegian fjords. This last example relates very well with issues addressed in this paper. The first question that arises relates to how a nonlinear wave, such as a solitary wave, goes through a sharp-bend (i.e. turn) of a channel. How much reflection is generated at this point where there is a sharp change in direction? This was addressed in 1992 by Harbitz [8] and in 1998 by Shi, Teng and Wu [17]. They identified that one parameter played a major role in the reflection characteristics. Namely the ratio *channel-width-to-wavelength*, which determines if a channel is narrow or wide. It was also observed that solitary waves shed very little reflection going through a narrow sharp-bend, as opposed to wider channels where a

reflected wave is clearly observed. These characteristics were reported but not explained. In the present work we rationalize why this is the case. Namely using a conformal mapping technique we are able to explain why solitary waves propagate easily through a narrow sharp corner.

Another problem of interest is the presence of a branching point in a channel. This configuration is also frequent in the examples given above. With respect to the problem of the Norwegian tsunamis, we point out that these fjords are in a very intricate domain where each individual branch makes sharp turns and also branches out into ramifications. Avalanches are common in these fjords. Huge rocks can fall and generate large waves that propagate for large distances through the intricate fjord network. Data indicates that the run-up of these waves, along the shoreline of the fjords, can be of several tens of meters. Results for a simulation of a rock slide, which confirms the data, were obtained through Dr. Carl Harbitz of the Norwegian Geotechnical Institute (NGI). See Fig. 1 where one finds nontrivial surface elevation along a big extent of the fjord network. One can also see the effect of having narrow and wide channels in the network. In [9] we indicate a link to the NGI where there is more information on the monitoring and modeling of the Åknes region. One will also find a report regarding the Åkne tsunami of 1934 which propagated for large distances and had a large run-up along the sides of the fjords, killing about 40 people [10]. In the link provided in [10] one can see photographs of a village that was destroyed by this 1934 tsunami. By clicking on the photograph one can see the village before and after the disaster.

Our goal is to better understand the dynamics of solitary waves in domains such as these intricate fjords. In particular the wave characteristics at sharp-bends and also at branching points. Our ultimate goal is to have a reliable one-dimensional reduced model that captures the main features of wave reflection and transmission in these types of domains. A schematic illustration with both the two-dimensional and the reduced (one-dimensional) domains is given in Fig. 2. This will lead to an efficient tool for these applications. Moreover, this class of problems will lead to new mathematical modeling and theory. To the best of the

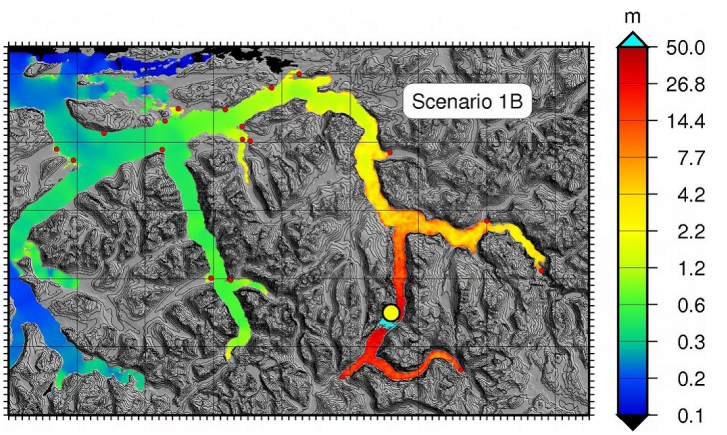

Fig. 1. Maximum surface elevation for a rock slide at Åknes (indicated by the large dot) of 45 million m^3 (logarithmic scale on the right). All the smaller dots indicate the most exposed villages for which were performed more detailed inundation studies. From NGI (2010) [15].

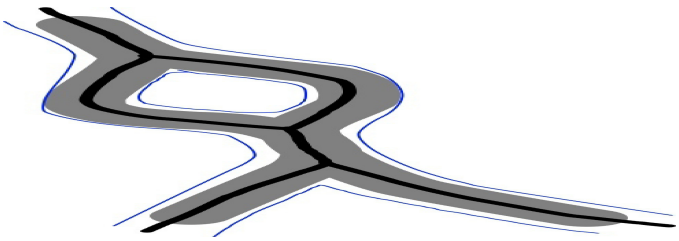

Fig. 2. Schematic illustration of configurations of interest: in *gray* the two-dimensional open channel with branching configurations; in a *black solid line* the reduction to a graph-like one-dimensional domain.

authors' knowledge, one cannot find much reference to this problem in the literature. Of particular interest is the question of compatibility conditions at the branching points, when the dynamics is governed by a Boussinesq-type system of partial differential equations.

In this paper we revisit the numerical simulations of [16, 17]. Based on their numerical method we present a new efficient algorithm to numerically solve the problem, in much more general channel configurations. The numerical method, that is reported to take hours, now takes a few minutes. We also present a new strategy to deal with the geometrical singularity due to corners at the sharp-bends. These novelties are based on the Schwarz–Christoffel transformation. Through a conformal mapping we perform our computations in a canonical domain, namely a uniform strip, having a variable coefficient (the Jacobian) and double-faced slits (in the case of branching points). An important improvement is that we are able to accurately impose the Neumann condition along the sides of the branching channel's reaches at arbitrary angles. Moreover, using the Jacobian of the Schwarz–Christoffel transformation we can rationalize the solitary wave characteristics at sharp-bends, both in the narrow and wide channel configurations. We also have an ongoing work on the effect of the Jacobian at branching points. Through this study we hope to understand how to deduce accurate reduced (one-dimensional) models for the reflection and transmission of solitary waves on graphs/networks. To the best of our knowledge this has not been done.

As a brief review of the literature we start by mentioning the work by Jacovkis [11]. In this work Jacovkis studies a one-dimensional hydrodynamic model for flows in complex networks, by considering the Saint Venant model. The underlying model is a linear hyperbolic model, where compatibility conditions at junctions are studied by using the method of characteristics. As expected, the necessary compatibility conditions depend on whether the flow is subcritical or supercritical. Extensions are proposed for systems with more than two equations in order to incorporate other modeling issues such as mobile (erodible) beds.

In 1992 Harbitz [8] considered solitary waves in L-shaped and expanding channels, as well as with T-shaped branching points. In 1998 Shi, Teng and Wu [17] considered the propagation of nonlinear waves in highly curved shallow water channels of constant depth and width. Both investigations were carried out through numerical simulations based on the generalized weakly nonlinear and weakly dispersive Boussinesq model [18]. Their goal was to investigate the effects of channel width and bending sharpness on the transmission and reflection of long waves propagating through significantly curved channels. It was found that when traveling through narrow channel bends, including both smooth and sharp-cornered 90°-bends, a solitary wave is transmitted almost completely with little reflection. On the other hand for solitary waves traveling through wide sharp-cornered 90°-bends,

wave reflection is significant. Their definition of narrow and wide channels will be made more precise in what follows.

More recently Shi, Teng and Sou [16] used the same model as in [17] to study solitary waves in branching channels. Due to the use of cartesian coordinates the numerical simulations with branching channels only consider reaches having angles which are multiples of 45°. This is so that the mesh points fall along the sides of the each reach. This helps to impose the Neumann condition along the side walls without having to interpolate for the corresponding velocity potential values.

This paper is organized as follows. In Sec. 2 we provide background material on the corresponding water wave problem. In Sec. 3 we describe how the Schwarz–Christoffel transformation plays a role in our formulation of sharp-bends. In Sec. 4 we describe the numerical method for solving the generalized Boussinesq system in curvilinear coordinates. We also present our new efficient algorithm that dramatically reduces computing time, together with numerical experiments involving sharp-bends and a preliminary branching channel experiment. In particular we show how the conformal mapping formulation is used to deal with artificial (numerical) spikes that appear near the inner corner's singular point. Finally in Sec. 5 we present our conclusions.

2. Background on the Water Wave Model

The surface water wave problem considered is governed by the three-dimensional Euler equations in the regime where the inviscid fluid flow is considered to be incompressible and irrotational. Details of the formulation are given in the article by Wu [18]. The Euler equations are formulated in the presence of free surface boundary conditions. Both the kinematic condition and a Bernoulli law are imposed along this free boundary. Under the assumption that the flow is considered to be incompressible and irrotational, a harmonic velocity potential $\Phi(x, y, z, t)$ is defined through which the velocity field can be obtained. In other words our notation is such that the velocity vector is denoted by $(U, V, W) = \nabla\Phi$ and the free surface wave elevation by $\eta(x, y, t)$. In order to make the free-boundary Euler equations more amenable for theoretical and numerical investigations Wu, in [18], deduced a Boussinesq system (in the horizontal x and y variables) by averaging the velocity potential over the depth. Let the channel be of depth h_o; then the reduced potential

$$\phi(x, y, t) = \frac{1}{h_o + \eta} \int_{-h_o}^{\eta} \Phi(x, y, z, t) dz$$

is used in the weakly nonlinear, weakly dispersive formulation for surface waves. In other words, in this wave-regime, Wu obtained the generalized Boussinesq system

$$\eta_t + (1 + \eta)(\phi_{xx} + \phi_{yy}) + \eta_x\phi_x + \eta_y\phi_y = 0, \tag{2.1}$$

$$\phi_t + \eta + \frac{(\phi_x)^2 + (\phi_y)^2}{2} - \frac{\phi_{xxt} + \phi_{yyt}}{3} = 0. \tag{2.2}$$

The horizontal velocity field is obtained by $(u, v) = \nabla\phi$, where now $\nabla = (\partial x, \partial y)$. A Neumann condition for the reduced velocity potential is imposed along the boundaries of the channels; the side walls of the channel are impermeable and very high (no spilling is allowed out of the bed).

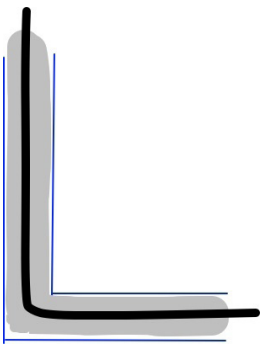

Fig. 3. Schematic illustration of a channel with an abrupt turn. In *gray* the top view of a two-dimensional open channel with a sharp-cornered 90°-bend; in the *black solid line* a schematic reduction to what would be a straight, variable coefficient, one-dimensional propagation medium.

Later in 1998, Wu and collaborators [17] explored these equations numerically regarding solitary waves in highly curved channels. A schematic configuration is presented in Fig. 3. The channel is considered to have a constant depth and a uniform rectangular cross section. In [17] the depth is set to 1 and also a boundary-fitted coordinate system is used to rewrite (2.1)–(2.2) so that channels with smooth curved walls can be analyzed. Abusing of notation, due to the change of variables given in [17], the Boussinesq system becomes

$$\eta_t + \frac{1}{L^2}[(1+\eta)\phi_x]_x + [(1+\eta)\phi_y]_y + \frac{\kappa}{L}(1+\eta)\phi_y = 0, \tag{2.3}$$

$$\phi_t + \eta + \frac{1}{2L^2}(\phi_x)^2 + (\phi_y)^2 - \frac{1}{3L^2}\phi_{xxt} - \frac{1}{3}\,\phi_{yyt} - \frac{\kappa}{3L}\phi_{yt} = 0. \tag{2.4}$$

where x is a coordinate tangential to the side walls, while y is normal to the side walls of the channel. For example, along a circular curve of the channel x plays the role of the angle θ while y of the radius r in a polar coordinate configuration (see [17, Fig. 1]). A similar formulation in curvilinear coordinates was presented for the (hyperbolic) Saint Venant equations by Fenton and Nalder in [3]. The curvature is denoted by κ while the scale factor L is $L = 1 + \kappa y$. This representation can be used for highly curved bends of the channel. The Neumann condition for the velocity potential is still trivially imposed along the boundaries of the channels. But if the channel has sharp corners this boundary-fitted coordinate system does not hold. Nevertheless the first set of experiments presented in [17] are for sharp-corned 90°-bends which can be done numerically with the original cartesian-coordinates formulation. Regarding Eqs. (2.3)–(2.4) the authors present an expression for the excess mass and the total mechanical energy. These quantities are monitored during their simulations [17] and shown to remain constant at an acceptable level.

Experiments for both sharp-corned 90°-bends as well as smooth, but significantly bent, channels are reported. In particular it is reported that the reflection and transmission properties of solitary waves going through these bends is mostly controlled by the ratio *width-to-wavelength*. Namely let b be the width of the channel while λ_e be the solitary wave's effective support (to be made more precise below). When b/λ_e is small the channel is *narrow* while when b/λ_e is not small the channel is *wide*. One way to make a distinction between the two regimes is when the reflection pattern changes. In [17] the authors report

that in narrow channels a solitary wave makes sharp turns more easily, namely with no reflection. To us this was a surprising fact. As mentioned in Sec. 1, one of the goals of this work is to rationalize the different solitary wave reflection regimes, regarding narrow or wide channels. This was not done in previous works.

As will be shown in subsequent sections, a conformal mapping change of variables plays an important role in rationalizing the reflections of solitary waves at narrow bends, as well as having nice properties regarding the numerical modeling. Note that using the Schwarz–Christoffel mapping [2, 14] both the smooth and sharp-corned 90°-bends are taken care of analytically, in our new formulation.

3. The Schwarz–Christoffel Transformation of Sharp-Corned Bends

We start with the generalized Boussinesq system (2.1)–(2.2). Shi *et al.* [17] solved this system numerically for a channel with a sharp-cornered 90°-bend. Namely in an L-shaped domain as in Fig. 3. This domain can be mapped onto a flat strip through the Schwarz–Christoffel mapping, which is tailored for polygonal-shaped regions [2]. Let the L-shaped domain/strip be defined in the complex z-plane, where $z = x + iy$. Hence there exists a Schwarz–Christoffel mapping from a flat strip in the (canonical) w-plane onto the L-shaped strip. Let $w = \xi + i\zeta$ and the Jacobian of the transformation be denoted by $|J| \equiv y_\xi^2 + y_\zeta^2 = |dz/dw|^2$. For the L-shaped domain the mapping $z = f(w)$ has singularities at the corners of the 90°-bend but is analytic otherwise. At one corner the Jacobian is zero (i.e. the mapping is not conformal) while at the other corner it blows up [2]. So in our formulation we trade geometric singularities for algebraic ones. But we will have a more general formulation by accommodating a wider range of channel configurations. Note that if the channel has no corners, the Jacobian is smooth in the whole domain since f is an analytic function.

Another way of thinking of the Schwarz–Christoffel (or the regular conformal) mapping is that the Boussinesq system can be reformulated in a new coordinate system, namely an orthogonal curvilinear coordinate system which is boundary fitted. In a wide range of non-smooth channel configurations, the Neumann condition along the side walls of the channel is easily imposed in the curvilinear coordinate system.

Another great advantage of the Schwarz–Christoffel mapping is that it applies also to branching channels, as will be shown below through an example. Hence, when compared to the analytical setup given in [16, 17], the present formulation accommodates for a much wider range of channel configurations altogether.

Recall the notation for the mapping f, namely that $z = f(w)$, where $w = \xi + i\zeta$. Then the generalized Boussinesq system now reads

$$\eta_t + \frac{(1+\eta)(\phi_{\xi\xi} + \phi_{\zeta\zeta})}{|J|} + \frac{\eta_\xi \phi_\xi + \eta_\zeta \phi_\zeta}{|J|} = 0, \tag{3.1}$$

$$\phi_t + \eta + \frac{\phi_\xi^2 + \phi_\zeta^2}{2|J|} - \frac{1}{3|J|}(\phi_{\xi\xi t} + \phi_{\zeta\zeta t}) = 0. \tag{3.2}$$

In the process of changing variables the following expressions are useful [14]:

$$\phi_x = \frac{1}{|J|}[x_\xi \phi_\xi + x_\zeta \phi_\zeta] \quad \text{and} \quad \phi_y = \frac{1}{|J|}[y_\xi \phi_\xi + y_\zeta \phi_\zeta],$$

together with the Cauchy–Riemann equations.

The conserved excess mass, due to the wave elevation, and the total energy are, respectively, given by

$$M(t) = \iint_\Omega \eta |J| d\xi d\zeta, \tag{3.3}$$

$$E(t) = \iint_\Omega \left(\frac{\eta^2 |J| + \phi_\xi^2 + \phi_\zeta^2}{2} \right) d\xi d\zeta. \tag{3.4}$$

The fluid domain is denoted by Ω. At rest these quantities are zero.

4. Numerical Method and Simulations

We adapt the Finite Difference Method used in [16, 17] for the generalized Boussinesq system in the $\xi\zeta$-coordinate system. First it is convenient to put all time derivatives in the left-hand side of the system:

$$\eta_t = -\frac{1}{|J|}[(1+\eta)(\phi_{\xi\xi} + \phi_{\zeta\zeta}) + (\eta_\xi \phi_\xi + \eta_\zeta \phi_\zeta)], \tag{4.1}$$

$$\left(\phi - \frac{\phi_{\xi\xi} + \phi_{\zeta\zeta}}{3|J|} \right)_t = -\eta - \frac{(\phi_\xi)^2 + (\phi_\zeta)^2}{2|J|}. \tag{4.2}$$

Next, a few comments on the Jacobian. Only in very few cases the Schwarz–Christoffel transformation, from the canonical w-plane onto the physical z-plane, is known in closed form since one is lead to elliptic integrals. On the other hand the conformal transformation f has a simpler expression for its derivative, but that depends on the knowledge of the vertices' preimages in the w-plane. In the majority of cases these preimages have to be found numerically [2]. As mentioned above, recall that $|df/dw|^2 = |J|$. Hence, in presenting our numerical method, we assume that we already know the variable coefficient $|J| = |J|(\xi, \zeta)$, which is numerically evaluated through the Schwarz–Christoffel Toolbox (MATLAB) described in the book by Driscoll and Trefethen [2].

Given the potential $\phi(\xi, \zeta, t)$, approximations to its spatial derivatives are obtained using the following (centered) finite differences, denoted accordingly. Let $\phi^n(i, j)$ be the condensed notation for $\phi(\xi_i, \zeta_j, t^n)$, where (ξ_i, ζ_j) are mesh points. Then

$$d_\xi \phi^n := \frac{\phi^n(i+1, j) - \phi^n(i-1, j)}{2\Delta\xi} = \phi_\xi^n(i, j) + O(\Delta\xi^2), \tag{4.3}$$

$$d_\zeta \phi^n := \frac{\phi^n(i, j+1) - \phi^n(i, j-1)}{2\Delta\zeta} = \phi_\zeta^n(i, j) + O(\Delta\zeta^2), \tag{4.4}$$

$$d_\xi^2\phi^n := \frac{\phi^n(i+1,j) - 2\phi^n(i,j) + \phi^n(i-1,j)}{\Delta\xi^2} = \phi^n_{\xi\xi} + O(\Delta\xi^2), \tag{4.5}$$

$$d_\zeta^2\phi^n := \frac{\phi^n(i,j+1) - 2\phi^n(i,j) + \phi^n(i,j-1)}{\Delta\zeta^2} = \phi^n_{\zeta\zeta} + O(\Delta\zeta^2). \tag{4.6}$$

The evolution scheme used in [16, 17] is straightforward. We use the same predictor–corrector scheme so that we can compare our results with the above references. There seems to be room for numerical improvement, but it is worth pointing out that the traveling (solitary) waves considered in their study are numerically propagated without changing shape, and conserving energy, which is reassuring for this evolution scheme. The predictor–corrector scheme can be outlined as follows. Let the right-hand side of (4.1) be denoted by $E^n(i,j)$, the right-hand side of (4.2) be denoted by $G^n(i,j)$ and define an auxiliary function $F \equiv \phi - (\phi_{\xi\xi} + \phi_{\zeta\zeta})/(3|J|)$. Namely using the centered schemes above, let

$$E^n(i,j) = -\frac{1}{|J|}((1+\eta^n)\ (d_\xi^2\phi^n + d_\zeta^2\phi^n) + d_\xi\eta^n d_\xi\phi^n + d_\zeta\eta^n d_\zeta\phi^n),$$

$$F^n(i,j) = \phi^n - (d_\xi^2\phi^n + d_\zeta^2\phi^n)/(3|J|)$$

and

$$G^n(i,j) = -\eta^n - [(d_\xi\phi^n)^2 + (d_\zeta\phi^n)^2]/(2|J|).$$

The predictor scheme for the wave elevation and the auxiliary function is simply

$$\eta_0^{n+1}(i,j) = \eta^n(i,j) + \Delta t E^n(i,j), \tag{4.7}$$

$$F_0^{n+1}(i,j) = F^n(i,j) + \Delta t G^n(i,j). \tag{4.8}$$

These values provide an initial guess for the (implicit) corrector scheme.

Now, for $\mu \geq 1$, the corrector scheme is given as

$$\eta_\mu^{n+1}(i,j) = \eta^n(i,j) + \frac{\Delta t}{2}\big[E_{\mu-1}^{n+1}(i,j) + E^n(i,j)\big], \tag{4.9}$$

$$F_\mu^{n+1}(i,j) = F^n(i,j) + \frac{\Delta t}{2}\big[G_{\mu-1}^{n+1}(i,j) + G^n(i,j)\big]. \tag{4.10}$$

The parameter μ indicates the number of iterations/corrections made. These iterations are performed until

$$\frac{\max\big(\eta_\mu^{n+1} - \eta_{\mu-1}^{n+1}\big)}{\max\eta^0} < 10^{-5}.$$

Usually only two iterations are needed. After each iteration one needs to recover the potential ϕ_μ^{n+1} from the auxiliary function F_μ^{n+1}, since its value is needed to evaluate E_μ^{n+1} and G_μ^{n+1} for the next iterate. Recall from the definition above, that this amounts to solving the discrete elliptic problem

$$\phi^n - (d_\xi^2\phi^n + d_\zeta^2\phi^n) = 3|J|F^n, \tag{4.11}$$

with trivial Neumann boundary conditions $d\phi^n/d\zeta = 0$ along the walls. Note that, from the definitions (4.5) and (4.6), we are using the 5-point Laplacian. Therefore we have to solve a sparse linear system of equations. This can be done very efficiently in MATLAB by defining the (time independent) system's matrix A as being sparse and performing its LU decomposition once and for all. The system's matrix A arises from the left-hand side of (4.11). Moreover, since our numerical domain is highly elongated we number the mesh points running first over the channel's transverse direction. This keeps the bandwidth as small as possible. As an example the mesh used for the experiment of Fig. 7, with a wider channel, has 26 nodes in the transverse direction and 913 nodes along the propagation direction. Thus the elliptic problem leads to a matrix of about 24000×24000, but which is (very) sparse. MATLAB handles sparse matrices very efficiently, both with respect to memory and operations.

In [16, 17] the authors mention that the simulations are time consuming. In [17] the authors report using a Cray Supercomputer to solve the problem while in the more recent work [16] report using both a Cray and a personal computer. It is reported that a calculation performed on a PC can take from 4 to 34 hours. This is far beyond the few minutes (of the order of 3 min) our numerical strategy (using the auxiliary function) requires with MATLAB on a personal computer (Apple iMac). In [17] it is mentioned that "the values of ϕ at new time levels appear on both the left-hand side and the right-hand side of the equations". In both references it is reported that an iterative method is therefore used to solve an associated linear system regarding both the predictor and corrector scheme. Namely to recover the potential that appears in both sides. Our impression is that a great amount of computer time can be saved by avoiding the iterative solution of linear systems at *every time step*. We get around this by using the auxiliary function. Our strategy amounts to *only one linear system* that is numerically handled through a sparse LU decomposition, once and for all. Thus at each corrector step we recover ϕ, from the auxiliary function F, by efficient forward and backward substitutions through the (narrow-banded) LU decomposition.

In summary the discretization scheme for the derivatives, proposed in [16, 17], is the same as ours but with a different definition of the right-hand sides in the predictor and corrector schemes. Therefore the main differences regarding the numerical methods are itemized as follows: (A) by using the Schwarz–Christoffel mapping we have more ease for imposing the Neumann condition along side walls that do not match the x or y-axis; (B) we use a more natural, geometrical strategy, to take care of artificial spikes near the corner of a sharp-bend; (C) we adopt an efficient strategy for the solution of the linear system (4.11) which reduces computing time by a large amount. Item (C) has been addressed above. Points (A) and (B) will be addressed in more detail below.

4.1. *Solitary waves through sharp-cornered bends*

Shi, Teng and Wu [17] report certain features of an solitary wave propagating in an open channel with sharp-cornered bends. As mentioned earlier, they recast the generalized Boussinesq system for boundary-fitted coordinates. Their coordinate system is not conformal but suits very well, for example, channel configurations with significantly curved circular turns. For the non-smooth turns, such as the sharp 90°-bend, this coordinate system does not apply. Nevertheless they perform numerical simulations in both smooth and non-smooth

cases. It is reported that the parameter playing the major role in the reflection dynamics is b/λ_e. When b/λ_e is small the channel is taken to be *narrow* and when it is large the channel is *wide*. The reflection of solitary waves at bends is negligible when the channel is narrow, while it is nontrivial when the channel is wide. Moreover the reflection pattern changes as the *wave amplitude* parameter α increases.

Our first goal in this numerical study is to reproduce their results and also (most importantly) to *rationalize* why the parameter b/λ_e plays this important role in the reflection process. This was not addressed in [17].

First we simulated this sharp-bend problem in the cartesian coordinate system. Namely by using the generalized Boussinesq system given in (2.1)–(2.2) and using the iterative scheme for solving the linear system of equations, as in [16, 17]. Next we tested our approach of using the auxiliary function and the LU decomposition to improve computing time. A big decrease in computing time was observed with our strategy. In all cases we checked for mass and energy conservation. Both the solution profile and conserved quantities agreed well with those of [17]. In particular we also observed the important property reported in [17] regarding no solitary wave reflection in a narrow channel with a sharp-cornered 90°-bend.

The following step was to repeat these experiments with the generalized Boussinesq system in the curvilinear coordinate system generated by the Schwarz–Christoffel transformation. As expected, the results are the same and for this reason we only present our numerical experiments in this new configuration.

Consider the *approximate* solitary wave profile given by [16]

$$\eta(x,t) = \frac{\alpha \operatorname{sech}^2 \beta(x - x_0 - ct)}{1 + \alpha \tanh^2 \beta(x - x_0 - ct)},$$

where $\beta(\alpha) = \sqrt{3\alpha/4(1 + 0.68\alpha)}$ and x_0 is the initial solitary wave position. The wave speed is

$$c(\alpha) = \sqrt{\frac{6(1+\alpha)^2}{\alpha^2(3+2\alpha)}[(1+\alpha)\ln(1+\alpha) - \alpha]}.$$

For a straight channel, of uniform depth and width as considered in our study, this profile is a very good approximation of a traveling wave. This is illustrated in Fig. 4.

The effective wavelength λ_e of this solitary wave is defined in [16] as the interval within which the wave elevation is larger than 1% of its amplitude α. This is expressed as

$$\lambda_e(\alpha) = \frac{2}{\beta} \ln \frac{(1 + 0.01\alpha)^{1/2} + 0.99^{1/2}}{(0.01 + 0.01\alpha)^{1/2}}.$$

Based on this formula, $\lambda_e(0.1) = 22.2$ and $\lambda_e(0.3) = 13.2$.

Let $\alpha = 0.1$ and $b = 1, 3$ and 5. Consider the traveling wave propagating from left to right. The results for these three different channel widths are displayed in Figs. 5–7. It is clearly seen that in narrow channels negligible reflection takes place as the wave propagates through the sharp-bend. Hence the presence of the singularity in the flow domain did not affect the traveling wave. As the channel becomes wider a reflected wave is then observed. The wider the channel the more reflection is observed, as can be seen by comparing

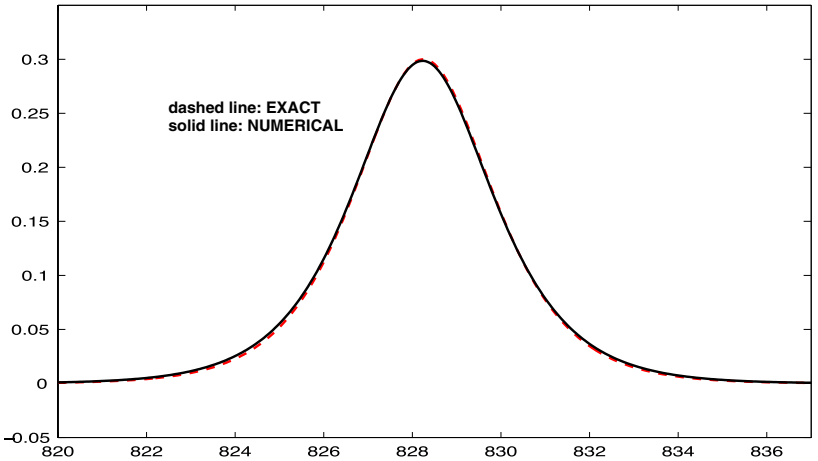

Fig. 4. Solitary wave ($\alpha = 0.3$) after propagating over a distance of approximately $60\lambda_e$. The relative error in speed was 0.0005, in amplitude was 0.005, in energy was 0.004 and in mass was 10^{-7}.

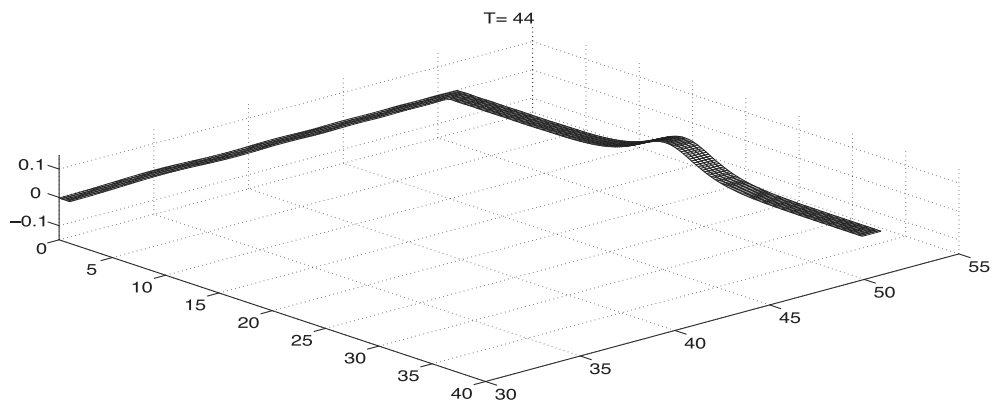

Fig. 5. Solitary wave after a sharp-cornered 90°-bend. Channel width is $b = 1$ and $\lambda_e \approx 22$.

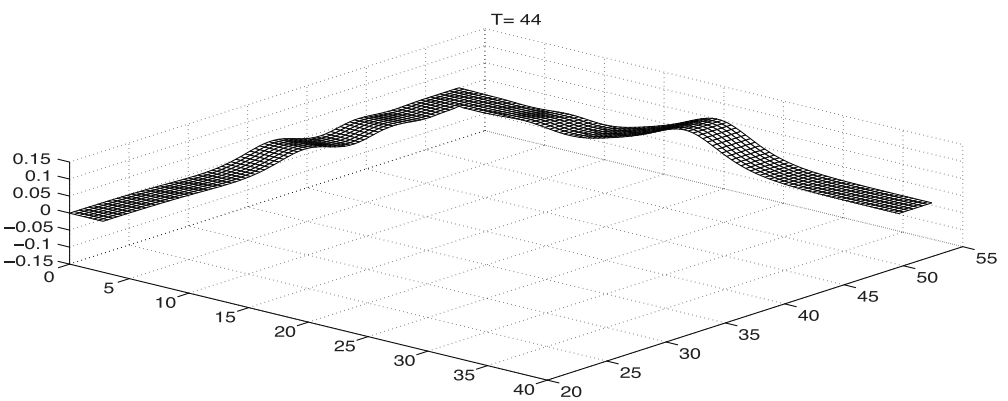

Fig. 6. Solitary wave after sharp-cornered 90°-bend. Channel width is $b = 3$ and $\lambda_e \approx 22$.

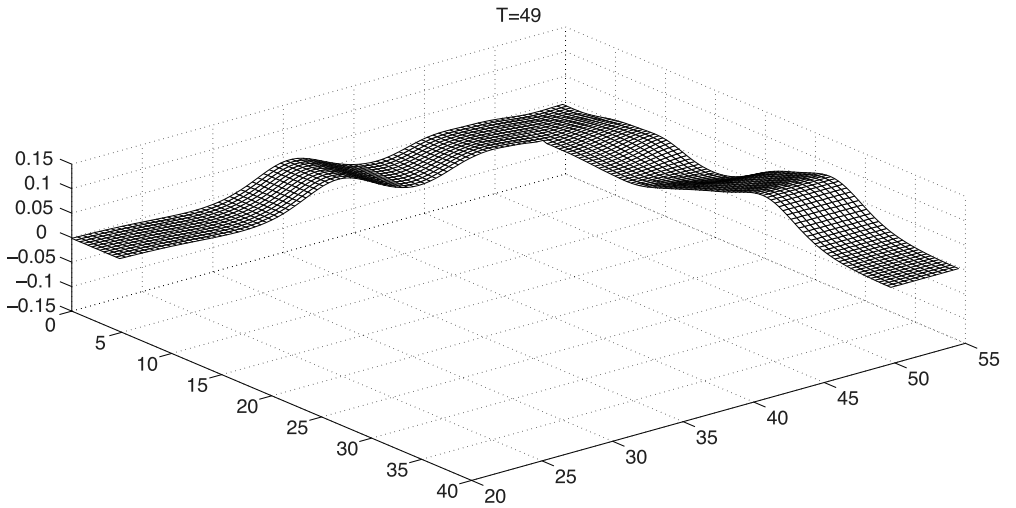

Fig. 7. Solitary wave after a sharp-cornered 90°-bend. Channel width is $b = 5$ and $\lambda_e \approx 22$.

Figs. 6 and 7. It is worth noting that the dynamics away from the corner is effectively one-dimensional. This observation is relevant regarding a one-dimensional reduced model.

We note that as we increase nonlinear effects through α, spurious spikes appear near the inner corner of the sharp-bend. Spikes of this nature are reported in [16] but not in [17]. We imagine it was also dealt with in the earlier publication [17].

In [16] the artificial spike was numerically addressed as follows. Consider the channel geometry as in Fig. 5. Let a denote the node at the inner corner. The velocity potential's value at this inner corner is calculated using the average of neighboring grid point values (denoted as $b \equiv$ north; $c \equiv$ east of a). In [16] the authors assume that $\phi_a = C_1\phi_b + C_2\phi_c$ and mention that while "testing for different values of C_1 and C_2, it was found that the value for ϕ_a affects the accuracy of mass and energy conservation quite significantly". Moreover they found that "for most cases, the values of C_1 and C_2 to minimize the errors were $C_1 \approx C_2 \approx 0.5$" and that "as long as the errors in mass and energy conservation are kept small, this localized small error does not affect the accuracy of the overall simulation significantly". Finally these authors make the comment that "For extremely narrow channels, the treatment is not perfect as some small artificial spikes of the wave elevation can still be seen near the corner point".

In our numerical experiments using the mapped domain, when the amplitude parameter is taken to be $\alpha = 0.1$, artificial spikes were not seen even in the narrow channel, as already shown in Figs. 5–7. But when the nonlinearity parameter was increased to the value used in [16], namely $\alpha = 0.3$ with $b = 3$, they appeared at the inner corner. The results are displayed in Figs. 8 and 9 and the artificial spikes are visible at the corner.

Through the use of the Schwarz–Christoffel mapping we are able to adopt an alternative (more geometrical and more natural) strategy to remove the spike. Instead of averaging the potential in an ad hoc fashion we gradually smooth the inner corner (only) by slightly modifying the mapping procedure. The impact of this strategy is clearly seen in Figs. 8 and 9, where the overall dynamics is unchanged, but the spike gradually disappears as we increase the inner corner's smoothing procedure as we now describe.

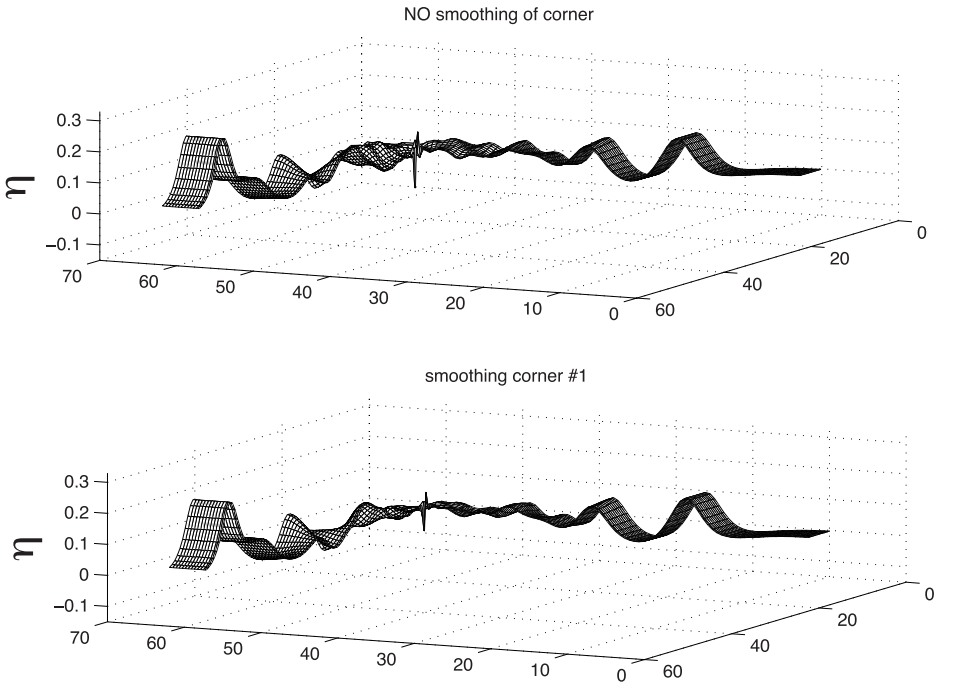

Fig. 8. Corner smoothing configurations. Channel width is $b = 3$ and $\lambda_e \approx 13$.

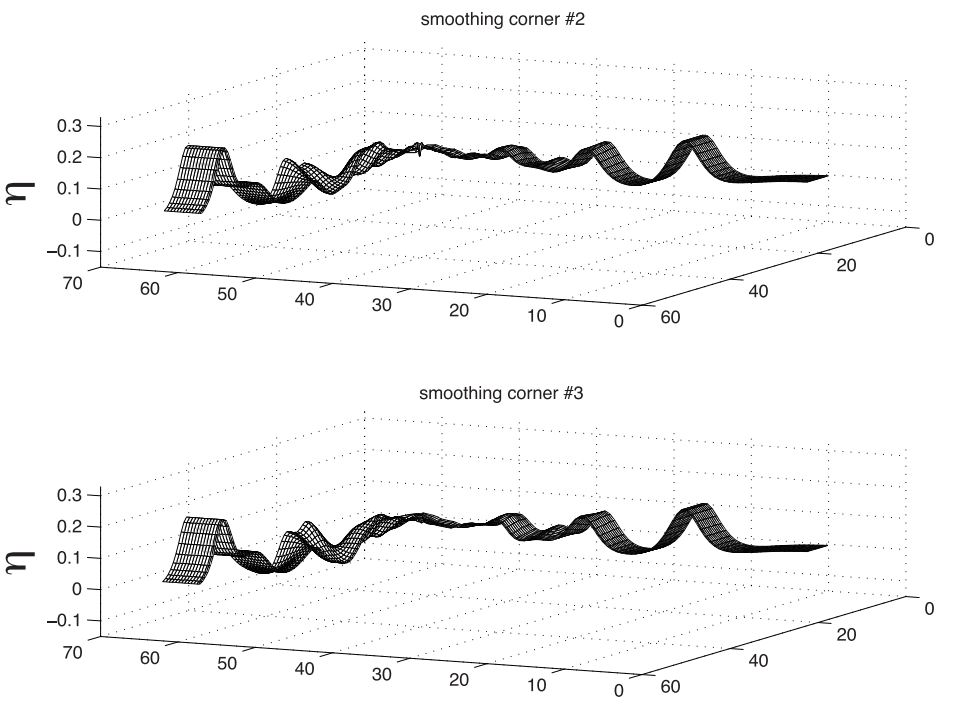

Fig. 9. Corner smoothing configurations. Channel width is $b = 3$ and $\lambda_e \approx 13$.

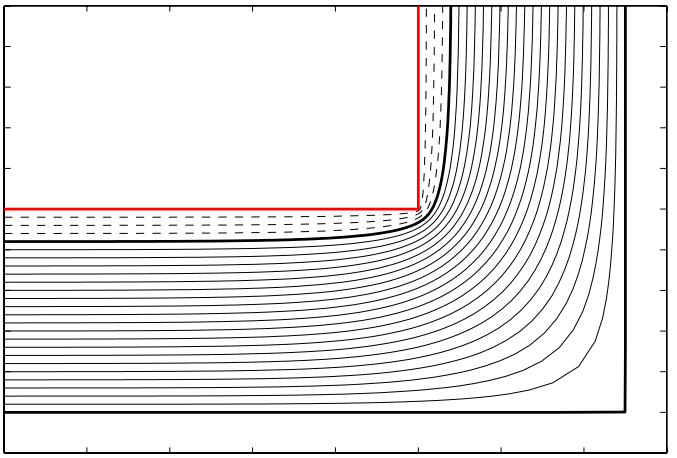

Fig. 10. Strategy for the smoothing of a sharp-cornered 90°-bend.

Notice that one can perform the Schwarz–Christoffel mapping from the uniform canonical strip onto a 90°-bent strip which is slightly wider than the physical channel. This is depicted in Fig. 10 where the corner has been reflected just for the sake of the smoothing discussion here presented. The flow domain is indicated by the domain with several level lines/curves expressed by different values of ζ equal to a constant. The bottom curve has a sharp corner indicating the outer corner, while the top level curve is the channel's wall, having a smoothed inner corner. The inner corner (outside the flow domain) is only considered for mapping purposes. Hence the dashed level curves are already outside the flow domain. Note that very quickly the inner wall of the channel becomes parallel to the outer wall, which still has a corner. In other words, this smoothing procedure amounts to putting the Jacobian's singularity near the inner wall of the channel, but outside the flow domain. In Fig. 11 we see the geometrical effect of pushing the Jacobian's singularity further away from the inner wall. Note that in Fig. 11 the length scale of the "shaved" corner, in all three cases, is quite small compared to the solitary wave's wavelength $\lambda_e = 13.2$. Nevertheless there is a local impact on the artificial spikes but not on the overall dynamics as shown in Figs. 8 and 9, which depict precisely each of these smoothing procedures.

4.1.1. *Rationalizing the wave-characteristics at sharp-bends*

Shi, Teng and Wu [17] reported that the parameter b/λ_e played a role in the reflection characteristics of a solitary wave propagating through a sharp-cornered 90^o-bend. They noticed that in the narrow-channel regime no reflection is observed. Even though there is a geometrical singularity in the flow domain, the long wave goes through this point retaining its traveling wave features. This remarkable fact was reported but not explained. Here we present one possible way to rationalize it.

Our formulation using the Schwarz–Christoffel mapping has proved to be useful in many ways. In this formulation the generalized Boussinesq system has a variable coefficient which is the Jacobian $|J|(\xi, \zeta)$. In other words, the dynamics is performed in the canonical domain (a straight channel) where the variable coefficient is responsible for producing reflections near the singular point, if that is the case. In Figs. 12 and 13 we display the Jacobian at

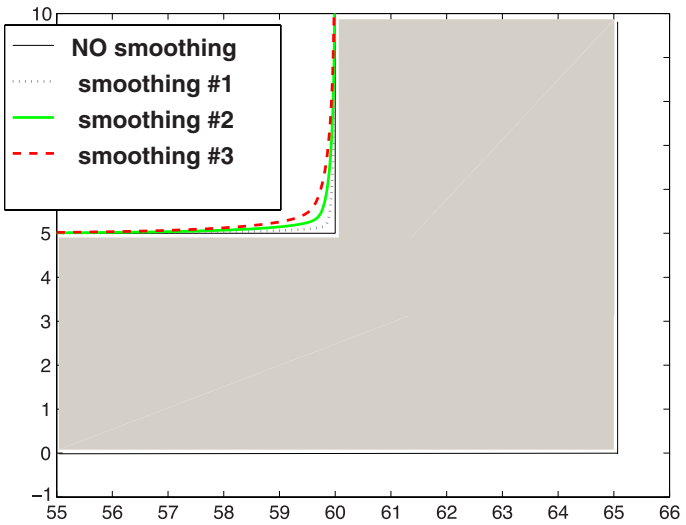

Fig. 11. The gray area is the flow domain near the sharp-corner. Different configurations for smoothed 90°-bends are displayed. These are the corresponding domains regarding the dynamics depicted in Figs. 8 and 9.

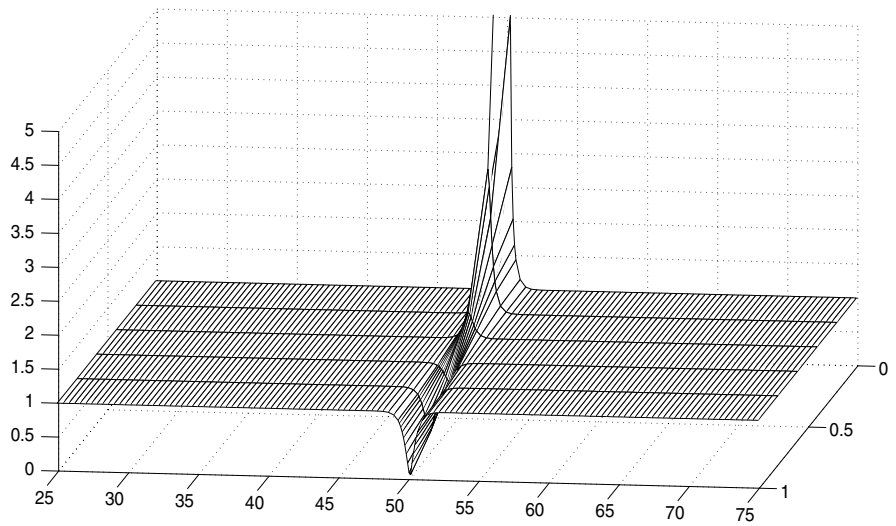

Fig. 12. Jacobian for a channel of width $b = 1$.

mesh points, for a channel of width $b = 1$ and $b = 5$, respectively. Take a long wave with $\lambda_e = 22.2$ ($\alpha = 0.1$). The Jacobian in the narrow ($b = 1$) case varies on a very short length scale regarding the solitary wave. Therefore these variations are not felt by the solitary wave and no reflected wave is produced near this point. On the other hand in the wider ($b = 5$) case the Jacobian varies over a larger interval and therefore interacts more with the solitary wave. In an analogy with topographies, for which one of the authors has a long experience [5–7, 12–14], long waves do not feel much a narrow (very localized) variation in the topography. Since most of the dynamics is nearly one-dimensional (certainly away from the corners) let us drop, for a moment, the ζ-variation in our generalized Boussinesq

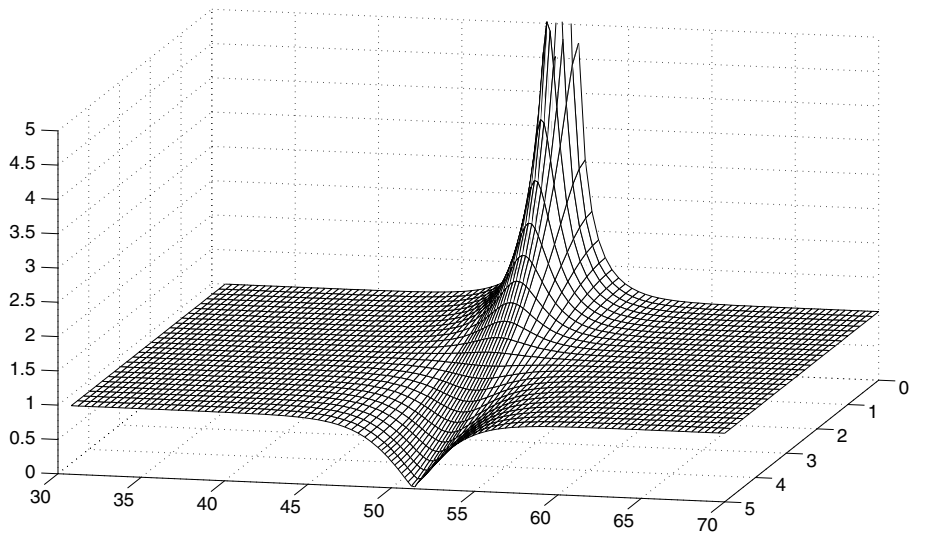

Fig. 13. Jacobian for a channel of width $b = 5$.

system. Namely one has that

$$\eta_t + \frac{[(1+\eta)\phi_\xi]_\xi}{|J|} = 0,$$

$$\phi_t + \eta + \frac{\phi_\xi^2}{2|J|} - \frac{1}{3|J|}\phi_{\xi\xi t} = 0.$$

We now compare with the one-dimensional terrain following Boussinesq system [14], while taking $\alpha = \beta = 1$ to simplify the comparison:

$$\eta_t + \frac{1}{|J|^{1/2}}\left[\left(1 + \frac{\eta}{|J|^{1/2}}\right)u\right]_\xi = 0,$$

$$u_t + \eta_\xi + \left(\frac{u^2}{2|J|}\right)_\xi - \frac{1}{3}u_{\xi\xi t} = 0,$$

where the conformal mapping was performed in the vertical direction rather than horizontally, as in this work. Recall that in the generalized Boussinesq system we can differentiate the second equation and set $\phi_\xi \equiv u$ to enhance the comparison. Even though these two Boussinesq systems are different, we can see some similarities that justify identifying bends with topographies. Both the presence of bends and topographies can generate reflected waves, depending on their associated length scales. And both these geometrical features can be encoded in a variable coefficient, through the Jacobian of the Schwarz–Christoffel mapping and the corresponding change of coordinates.

4.2. *Solitary waves propagating through branching points*

In [16] Shi, Teng and Sou study solitary waves through branching channels. The generalized Boussinesq system (2.1)–(2.2) is solved in cartesian coordinates with the same numerical

scheme as used in [17]. Their basic configuration studied, regarding the branching channel, consists of a primary straight channel and a secondary reach branching out at an angle θ. While the model is not restricted to any angle θ, the numerical simulations were performed for angles $\theta = 45, 90, 135$ degrees, since these angles are better adjusted to imposing the Neumann condition in the cartesian coordinates system. The authors compared their numerical simulations with laboratory experiments. Special attention is given to the transmission of a solitary wave through both a sharp-cornered 90°-bend and a right-angle branching channel. Good agreement is observed for these two cases. Branching points at 90° were also studied by Harbitz [8].

Again we point out that the Schwarz–Christoffel mapping can be used in this channel configuration. Moreover, under this mapping all branching-angle configurations can be easily dealt with, regarding the numerical method. The Neumann boundary condition along the side walls is easily imposed in the ζ-coordinate which is boundary fitted. In cartesian coordinates it is useful to choose Δx and Δy so that the grid points fall along the side walls of a branching reach. For example this happens when $\theta = 45$ and $\Delta x = \Delta y$. When the branching channel has a (symmetric) Y-configuration one could still play with the spatial mesh spacing in order to adjust for boundary conditions, but having a distorted mesh depending on the angle. But this mesh adjustment to the geometry will be lost for non-symmetric Y-configurations, where one reach has an angle θ_1 downwards and the other reach has an angle $\theta_2 \neq \theta_1$ upwards. In this case imposing the Neumann condition will be more complicated and, very likely, would require the use of interpolation.

At this time we have an ongoing study for branching channels in very general configurations. Our goal is to explore as many transmission and reflection regimes in order to rationalize its main features. In this process we are making progress in the direction of obtaining a reduced one-dimensional model for solitary waves on a graph (network). We will lose some information on the dynamics, as we perform the one-dimensional reduction, but we hope to retain some essential features in the reduced model, such as the bulk of water transmitted downstream. This is of great value for applications related to great disturbances in rivers, channel networks and tsunamis in fjords as described in Sec. 1. A reliable reduced one-dimensional model is by far more efficient for quickly predicting the bulk of water that will reach point A or B downstream.

Moreover from the mathematical point of view a one-dimensional reduced model also brings new theoretical challenges that apparently are not resolved in the literature. The first challenge, for which we have made some progress, is establishing a weakly nonlinear, weakly dispersive system of partial differential equations on graphs (networks) which supports the reflection and transmission of solitary waves. Furthermore, this model calls for mathematical analysis in providing further insight and rigor on, for example, obtaining compatibility conditions at the branching points. This is one of the many examples where analysis is extremely valuable. Recall that Jacovkis [11] has an article on the compatibility conditions for linear shallow water waves on graphs. It is based on the method of characteristics. Another reference to be mentioned is the work by Bona and Cascaval [1] where the Benjamin–Bona–Mahony (BBM) equation is considered. In [1, 11] the two compatibility conditions are connected with continuity of both the wave field and of flux conditions at the node. In [1] the authors discuss existence of solutions, and so on, in the presence of branching points. Analysis on the half-line and intervals is addressed by the

authors. The proposed application is for the flow in arteries. Unfortunately the BBM model being uni-directional does not account for reflected waves. Regarding flow in arteries, and other Bio-Math applications, a series of publications of interest is that of Quarteroni and collaborators. One reference that provides an overview of their work is [4].

As mentioned in Sec. 1, through the Schwarz–Christoffel mapping we perform our computations in the canonical domain, namely on a uniform strip having a variable coefficient (the Jacobian). In the case of a branching channel the canonical domain presents a double-faced slit. In Fig. 14 we present a symmetric Y-configuration, for the branching channel. The uniform mesh in the $\xi\zeta$-coordinates is graphed in the physical domain. The computational grid is depicted in Fig. 15, where it is clearly indicated that the slit is double-faced, namely by having a different node at each of its sides. Note that each side of the slit is on a different reach of the channel. An important improvement of this numerical setup is that we are able to accurately impose the Neumann condition along the sides of the branching channel's reaches at arbitrary angles.

We now provide a preliminary result for a solitary wave propagating through a branching point of a (symmetric) Y-configuration, with angles of 30° each. A snapshot is provided in Fig. 16. A solitary wave ($\alpha = 0.1$) propagates from the right to the left and meets the branching point in a channel of width $b = 1$. Due to the symmetric configuration the traveling wave breaks into two equal waves along each reach. Small oscillations are seen behind these waves. Most of the excess mass is contained in these waves. Nevertheless a reflected wave propagates back, to the right of the branching point. Our goal in this study is to rationalize the reflection–transmission mechanism's essential features in as many configurations we can, namely symmetric and non-symmetric branches. The conformal mapping is very convenient for this analysis because there is no angle restriction. Moreover, the Jacobian plays an important role in the rationalizing of the reflection–transmission mechanism.

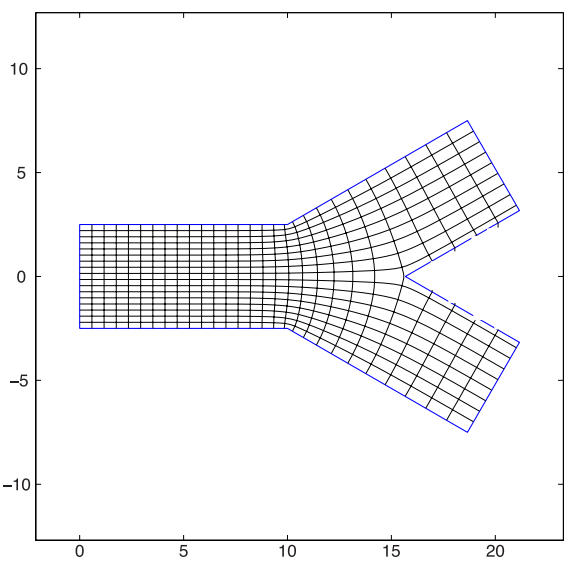

Fig. 14. Branching channel with a symmetric Y-configuration. The uniform grid in the w-plane (see Fig. 15) is mapped onto the physical domain. The mesh is boundary fitted and very quickly adjusts to a rotated cartesian grid, along each reach of the channel.

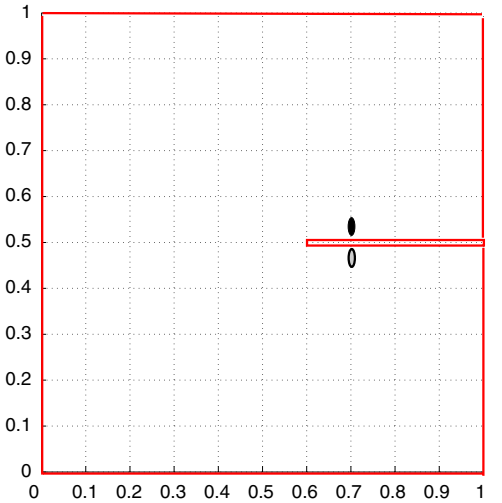

Fig. 15. Branching channel, with a symmetric Y-configuration (see Fig. 14), and its uniform grid in the canonical domain. The corresponding sides of the upper and lower reaches have as preimages the upper and lower sides of a slit. Two nodes are assigned at each point of the slit: one for the upper Neumann condition and the other for the lower Neumann condition.

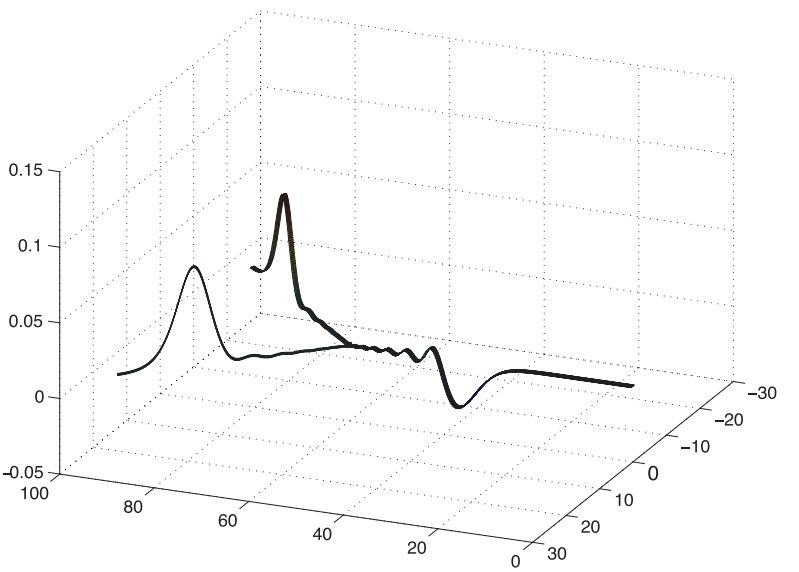

Fig. 16. Solitary wave ($\alpha = 0.1$) propagating from the right to the left, after passing through a branching point. A reflected wave is seen propagating back to the right. The branching point has a symmetric Y-configuration with $\theta_1 = \theta_2 = 30$.

5. Conclusion

Our goal was to study the dynamics of solitary waves in intricate domains having channels with sharp-bends and branching points. In particular we rationalized the wave characteristics at sharp-bends by using the Jacobian of the Schwarz–Christoffel transformation and observing that it acts in a similar way as a topography, as in [14]. We revisited previous numerical studies and presented a new efficient algorithm which computationally solves the

problem in much more general channel configurations. Reported numerical methods need hours to solve a problem, while now ours takes a few minutes. We also presented a new strategy to deal with the geometrical singularity due to corners at the sharp-bends. These novelties are also based on the Schwarz–Christoffel transformation.

Regarding future work and directions, we have an ongoing work on the effect of the Jacobian at branching points. Through this study we hope to understand how to deduce accurate reduced (one-dimensional) models for the reflection and transmission of solitary waves on graphs/networks. To the best of our knowledge this has not been done. Our ultimate goal is to have a reliable one-dimensional reduced model that captures the main features of wave reflection and transmission in these types of domains. This will lead to an efficient tool for these applications. Moreover, this class of the problems will lead to new mathematical modeling and theory. Of particular interest is the question of compatibility conditions at the branching points, when the dynamics is governed by a Boussinesq-type system of partial differential equations.

Acknowledgments

The authors would like to thank Dr. Carl Harbitz (NGI) for kindly allowing us to use Fig. 1 and also for pointing out the paper [8]. The work of Nachbin was supported in part by: CNPq under (PQ-1B) 454027/2008-7; and FAPERJ *Cientistas do Nosso Estado* project #102917/2011. The work of Simões was supported by the Brazilian National Petroleum Agency (ANP) through the program COMPETRO PRH32.

References

[1] J. Bona and R. C. Cascaval, Nonlinear dispersive waves on trees, *Canad. Appl. Math. Quart.* **16** (2008) 1–18.
[2] T. A. Driscoll and L. Trefethen, *Schwarz–Christoffel Mapping* (Cambridge University Press, 2002).
[3] J. D. Fenton and G. V. Nalder, Long wave equations for waterways curved in plan, in *26th Congr. of the Int. Association for Hydraulic Research* (London, 1995), pp. 573–578.
[4] L. Formaggia, D. Lamponi and A. Quarteroni, One-dimensional models for blood flow in arteries, *J. Eng. Math.* **47** (2003) 251–276.
[5] J.-P. Fouque, J. Garnier, J. C. Muñoz-Grajales and A. Nachbin, Time-reversing solitary waves, *Phys. Rev. Lett.* **92** (2004) 094502.
[6] J.-P. Fouque, J. Garnier and A. Nachbin, Shock structure due to stochastic forcing and the time reversal of nonlinear waves, *Physica D* **195** (2004) 324–346.
[7] J. Garnier, R. A. Kraenkel and A. Nachbin, Optimal Boussinesq model for shallow-water waves interacting with a microstructure, *Phys. Rev. E* **76** (2007) 046311.
[8] C. B. Harbitz, Reflection-transmission of nonlinear waves in channel bends, preprint, Institute of Mathematics, University of Oslo, Norway, No. 6 (April, 1992).
[9] http://www.ngi.no/en/Contentboxes-and-structures/Reference-Projects/...Reference-projects/Monitoring-and-modelling-of-the-Aknes/.
[10] http://www.tu.no/nyheter/naturvitenskap/2005/01/11/norske-tsunamier.
[11] P. M. Jacovkis, One-dimensional hydrodynamic flow in complex networks and some generalizations, *SIAM J. Appl. Math.* **51** (1991) 948–966.
[12] J. C. Muñoz and A. Nachbin, Stiff microscale forcing and solitary wave refocusing, *SIAM Multi. Model. Simul.* **3** (2005) 680–705.
[13] J. C. Muñoz and A. Nachbin, Improved Boussinesq-type equations for highly-variable depths, *IMA J. App. Math.* **71** (2006) 600–633.

[14] A. Nachbin, A terrain-following Boussinesq system, *SIAM J. Appl. Math.* **63** (2003) 905–922.
[15] NGI, The Åknes/Tafjord project, Numerical simulations of tsunamis from potential and historical rock slides in Storfjorden; Hazard zoning and comparison with 3D laboratory experiments, Report 20051018-00-1-R Rev. 01, Norwegian Geotechnical Institute (21 February 2011).
[16] A. Shi, M. H. Teng and I. M. Sou, Propagation of solitary waves in branching channels, *ASCE J. Engng. Mech.* **131** (2005) 859–871.
[17] A. Shi, M. H. Teng and T. Y. Wu, Propagation of solitary waves through significantly curved shallow water channels, *J. Fluid. Mech.* **362** (1998) 157–176.
[18] T. Y. Wu, Long waves in ocean and coastal waters, *ASCE J. Engng. Mech.* **107** (1981) 501–522.